Shell Model FEM Analysis of Buried Pipelines under Seismic Loading

AUTHOR(S):

YANG, Rihui; KAMEDA, Hiroyuki; TAKADA, Shiro

Bull. Disas. Prev. Res. Inst., Kyoto Univ., Vol. 38, Part 3, No. 336, June, 1988

Shell Model FEM Analysis of Buried Pipelines under Seismic Loading

By Rihui YANG, Hiroyuki KAMEDA and Shiro TAKADA

(Manuscript received June 15, 1988)

Abstract

This paper presents the development of an FEM formulation based on shell Models for the analysis of buried pipelines subjected to sinusoidal seismic wave, differential settlement and dislocation of ground. Realistic circumferential distribution of earth pressure and distortion of the cross section of the pipe, which can not be considered in the conventional method based on the beam model, were taken into consideration. Some comparison of numerical results obtained from the shell model-I, shell model-II and the beam model[1] is carried out. It is found that very different axial stresses were given by each of the three models in the case of transverse ground deformation, and it is apparent that beam model and shell model-I are not suitable in such cases. Distortion of the cross section of pipes does occur in the case of stiff ground or thin pipes, which may make the circumferential stress become more significant than the axial stress. An empirical formula is presented to evaluate the ratio of axial stress obtained from these shell models.

1. Introduction

1.1. Previous Works on Buried Pipelines

The behavior of buried pipelines during an earthquake is a problem which has attracted considerable attention due to its importance and the great potential for desrubtion of lifeline service. A great deal of work has been done in the last decade. This may be divided into the following four areas.

(1) Investigation and analysis of the past earthquake damage data.
(2) Investigation and analysis of seismic environment, which includes the characterization of input seismic traveling wave, liquefaction, differential settlement, landslide and faulting.
(3) Theoretical and experimental analyses of physical pipeline components under seismic loading.
(4) System reliability and risk analysis by means of network theory and probability theory.

The apparent mechanism of response and failure of pipeline components is the fundamental problem and the reliable result of the system reliability and risk analysis depends to a great extent on how well physical component behavior is understood. Nevertheless, it appears that more work has been done on the area (4) in the past several years, while further study on the area (3) is obviously necessary. In the light

of this situation, a new analysis method of component behavior during an earthquake is presented in this paper.

1.2. Models for Analysis of Buried Pipes

Up to the present, there have been three kinds of models used to simulate the interaction of pipes and ground. These are the beam model, lumped mass model and shell model.

The beam model is a conventional model and has been used in most of the analyses which treat the ground-pipeline interaction system as a beam embedded in an infinite isotropic homogeneous elasto-plastic medium or surrounded by soil springs. Usually the problem is treated as a quasi-static one by dropping the intertial and damping terms in the governing differential equations. S. Takada[1),2)], M. Shinozuka and T. Koike[3),4)] have been successful in using this kind of model.

In order to consider the inertial and damping effects, a lumped mass-spring-dashpot system was presented by M. Novak et al[5)]. They concluded that dynamic pipe-ground interaction reduces pipe stress but this reduction is significant only for very soft soils and resonance type amplification does not occur.

S. K. Datta et al. modeled the pipe-ground system as a thin cylindrical shell embedded in an infinite isotropic homogeneous elastic medium in the case of axisymmetric loading. Numerical response analysis of a buried pipe due to an axial compressional wave showed that the dynamic response of pipeline was significantly altered by the changes in the Poisson's ratio and the rigidity modulus of the surrounding medium, but pipe resonance occurred only when the rigidity ratio was large and the wave length was small [6, 7, 8].

The beam model and lumped mass model treat the pipes as beams or masses, thus the real distribution of earth pressure and the distortion of the pipe cross section can not be considered. The circumferential stress of pipes can not be evaluated either. To solve these problems, the shell model was used in this study. We adopted the matrix displacement method[10),11),12),13)] for numerical calculation, which made the analysis of asymmetric loadings possible.

2. Shell Models and Numerical Computational Method

2.1. Matrix Displacement Method for Analysis of Shell of Revolution

General View

It is well known from the thin shell theory that if loadings (body forces or surface tractions) are axisymmetric, then the responses (displacements, stresses, etc.) are also axisymmetric ; if loadings are distributed as a sine or cosine function along the circumference, the responses are also distributed in the same way along that direction. Thus, it is only necessary to consider the amplitudes in analysis. For an asymmetric loading, it is only necessary to expand the loading into a Fourier series, calculate responses to each Fourier term and superpose them, then we obtain the responses to the loading. This

is the basic concept of the matrix displacement method.

Coordinate System, Generalized Nodal Displacements and Forces of an Element e_{ij}

In **Fig. 1** an arbitrary element e_{ij} in the cylindrical coordinates that is employed in the analysis is illustrated. The generalized displacements and forces of an arbitrary nodal circle i are given by

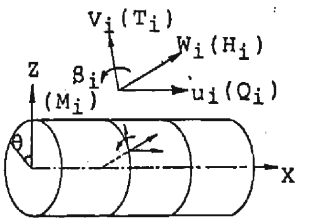

Fig. 1 Elements in a generalized coordinate system.

$$\{d_i\} = \{u_i,\ v_i,\ w_i,\ \beta_i\}^T$$
$$\{f_i\} = \{Q_i,\ T_i,\ H_i,\ M_i\}^T \tag{1}$$

in which u_i, v_i, w_i are displacements in axial, circumferential and radial directions, respectively. V_i, T_i, and H_i are forces in these directions. M_i, β_i are moment and the rotational angle about the tangent to the nodal circle. The generalized nodal forces and displacements corresponding to an arbitrary term in a loading Fourier series expansion are expressed in the following. Displacements are written as

$$\{d_i\} = [u_{in}(x)\cos n\theta,\ v_{in}(x)\sin n\theta,\ w_{in}(x)\cos n\theta,\ \beta_{in}(x)\cos n\theta]^T \tag{2}$$

Their amplitudes are

$$\{d_{in}\} = [u_{in}(x),\ v_{in}(x),\ w_{in}(x),\ \beta_{in}(x)]^T \tag{3}$$

Forces are given by

$$\{f_i\} = [Q_{in}(x)\cos n\theta,\ T_{in}(x)\sin n\theta,\ H_{in}(x)\cos n\theta,\ M_{in}(x)\cos n\theta]^T \tag{4}$$

Their amplitudes are

$$\{f_{in}\} = [Q_{in}(x),\ T_{in}(x),\ H_{in}(x),\ M_{in}(x)]^T \tag{5}$$

Since only the amplitudes are considered in the following deduction and calculation, we will use them to describe displacements, forces, stresses, etc. and not specifically say that they are amplitudes, but readers will readily recognize them as such from their subscript. Therefore, the generalized nodal displacements of an arbitrary element e_{ij} can be written as

$$\{d_{ijn}\} = [u_{in}(x),\ v_{in}(x),\ w_{in}(x),\ \beta_{in}(x),\ u_{jn}(x),\ v_{jn}(x),\ w_{jn}(x),\ \beta_{jn}(x)]^T \tag{6}$$

Corresponding generalized nodal forces are given by

$$\{f_{ijn}\} = [Q_{in}(x), T_{in}(x), H_{in}(x), M_{in}(x), Q_{jn}(x), T_{jn}(x), H_{jn}(x), M_{jn}(x)]^T \tag{7}$$

Displacement Assumption

Displacements in element e_{ij} can be expressed as

$$\{u_n\} = [u_n(x),\ v_n(x),\ w_n(x),\ \beta_n(x)]^T \tag{8}$$

Assume the displacements to be polynomial functions of axial coordinates, that is

$$\{u_n\} = \begin{Bmatrix} u_n \\ v_n \\ w_n \\ \beta_n \end{Bmatrix} = \begin{bmatrix} 1 & \xi & 0 & 0 & 0 & 0 & 0 & 0 \\ 0 & 0 & 1 & \xi & 0 & 0 & 0 & 0 \\ 0 & 0 & 0 & 0 & 1 & \xi & \xi^2 & \xi^3 \\ 0 & 0 & 0 & 0 & 0 & 1/L & 2\xi/L & 3\xi^2/L \end{bmatrix} \begin{Bmatrix} a_1 \\ a_2 \\ \cdots \\ a_8 \end{Bmatrix} \tag{9}$$

where $\xi = S/L$ is a dimensionless axial coordinate, and s is the distance from nodal circle i to the circle considered. Substitute the boundary condition

$$\{u_n\}_{\xi=0} = \{d_{in}\} \qquad \{u_n\}_{\xi=1} = \{d_{in}\} \tag{10}$$

into equation (9), and coefficients a_m, $m = 1, 2, \ldots, 8$ can be calculated. After substitution of a_m into Eq. (9), the amplitudes of generalized displacements are given by

$$\begin{Bmatrix} u_n \\ v_n \\ w_n \\ \beta_n \end{Bmatrix} = \begin{bmatrix} 1-\xi & 0 & 0 & 0 & \xi & 0 & 0 & 0 \\ 0 & 1-\xi & 0 & 0 & 0 & \xi & 0 & 0 \\ 0 & 0 & 1-3\xi^2+2\xi^3 & L(\xi-2\xi^2+\xi^3) & 0 & 0 & 3\xi^2-2\xi^3 & -L(\xi^2-\xi^3) \\ 0 & 0 & -6(\xi-\xi^2)/L & 1-4\xi+3\xi^2 & 0 & 0 & 6(\xi-\xi^2)/L & -2\xi+3\xi^2 \end{bmatrix} \begin{Bmatrix} u_{in} \\ v_{in} \\ w_{in} \\ \beta_{in} \\ u_{jn} \\ v_{jn} \\ w_{jn} \\ \beta_{jn} \end{Bmatrix} \tag{11}$$

or

$$\{u_n\} = [N]\{d_{ijn}\}$$

Strain-Displacement Relations

The strain-displacement relations of a thin shell are expressed as[8]

$$\left.\begin{aligned} \varepsilon_x &= \frac{\partial u}{\partial x} \\ \varepsilon_\theta &= \frac{1}{r}\frac{\partial v}{\partial \theta} + \frac{w}{r} \\ \varepsilon_{x\theta} &= \frac{1}{r}\frac{\partial v}{\partial \theta} + \frac{v}{x} \\ \kappa_x &= -\frac{\partial w^2}{\partial x^2} \\ \kappa_\theta &= -\frac{1}{r}\frac{\partial^2 w}{\partial \theta^2} + \frac{1}{r^2}\frac{\partial v}{\partial \theta} \\ \kappa_{x\theta} &= 2\left(-\frac{1}{r^2}\frac{\partial^2 w}{\partial x \partial \theta} + \frac{1}{r}\frac{\partial v}{\partial x}\right) \end{aligned}\right\} \tag{12}$$

or in matrix form

$$\begin{Bmatrix} \varepsilon_x \\ \varepsilon_\theta \\ \varepsilon_{x\theta} \\ \kappa_x \\ \kappa_\theta \\ \kappa_{x\theta} \end{Bmatrix} = \begin{bmatrix} \frac{\partial}{\partial x} & 0 & 0 & 0 \\ 0 & \frac{1}{r}\frac{\partial}{\partial \theta} & \frac{1}{r} & 0 \\ \frac{1}{r}\frac{\partial}{\partial \theta} & \frac{\partial}{\partial x} & 0 & 0 \\ 0 & 0 & \frac{\partial^2}{\partial x^2} & 0 \\ 0 & \frac{1}{r^2}\frac{\partial^2}{\partial \theta^2} & \frac{-1}{r^2}\frac{\partial}{\partial \theta} & 0 \\ 0 & \frac{2}{r}\frac{\partial}{\partial x} & \frac{-1}{r}\frac{\partial^2}{\partial x \partial \theta} & 0 \end{bmatrix} \begin{Bmatrix} u \\ v \\ w \\ \beta \end{Bmatrix} \tag{13}$$

in which ε_x, ε_θ, $\varepsilon_{x\theta}$ are strain components and κ_x, κ_θ, $\kappa_{x\theta}$ are changes of curvatures in the middle surface. Also only the amplitudes are necessary. They are

$$\{\varepsilon_n\} = [\varepsilon x_n(x),\ \varepsilon\theta_n(x),\ \varepsilon_{x\theta n}(x),\ \kappa_{xn}(x),\ \kappa_{\theta n}(x),\ \kappa_{\theta xn}(x)]^T \tag{14}$$

Using Eqs. (8), (11) and (12), the strains of the middle surface are readily deduced as

$$\{\varepsilon_n\} = [B]\{d_{ijn}\} \tag{15}$$

in which $[B]$ is a 6*8 matrix (see Eq. $(A-1)$ in a appendix A)

Generalized Hooke's Law

Membrane stress resultants and moment resultants are adopted in the analysis. The directions of these force resultants in an element are shown in **Fig. 2,** in which we

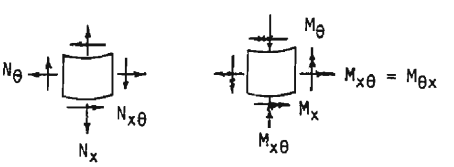

Fig. 2 Directions of generalized force resultants.

have neglected transverse-shear resultants N_{xz} and $N_{\theta z}$ which are less important when evaluating work or energy, but is necessary when considering the equilibrium. In that sense, the force resultant can be written as

$$\{\sigma_n\} = [Nx_n(x),\ N_{\theta n}(x),\ N_{z\theta n}(x),\ M_{xn}(x),\ M_{\theta n}(x),\ M_{\theta xn}(x)]^T \tag{16}$$

The generalized Hooke's law here becomes[8]

$$\begin{Bmatrix} N_{xn} \\ N_{\theta n} \\ N_{x\theta n} \\ M_{xn} \\ M_{\theta n} \\ M_{x\theta n} \end{Bmatrix} = \frac{Eh}{1-\nu^2} \begin{bmatrix} 1 & y & 0 & 0 & 0 & 0 \\ y & 1 & 0 & 0 & 0 & 0 \\ 0 & 0 & (1-\nu)/2 & 0 & 0 & 0 \\ 0 & 0 & 0 & h^2/12 & \nu h^2/12 & 0 \\ 0 & 0 & 0 & \nu h^2/12 & h^2/12 & 0 \\ 0 & 0 & 0 & 0 & 0 & (1-\nu)h^2/24 \end{bmatrix} \begin{Bmatrix} \varepsilon_{xn} \\ \varepsilon_{\theta n} \\ \varepsilon_{x\theta n} \\ \kappa_{xn} \\ \kappa_{\theta n} \\ \kappa_{x\theta n} \end{Bmatrix} \tag{17}$$

or

$$\{\sigma_n\} = [D]\{\varepsilon_n\}$$

Virtual Displacement Principle

Consider an element e_{ij}, assuming that inertial and damping effects are negligible. By using the virtual displacement principle, we have

$$\delta w = -\int_V \delta\{\varepsilon\}^T\{\sigma\}dv + \int_V \delta\{u\}^T\{f_b\}dv + \int_s \delta\{u\}^T\{f_s\}ds = 0 \tag{18}$$

Then,

$$-\int_0^{2\pi}\int_0^L \delta\{\varepsilon\}^T\{\sigma\}rdsd\theta + \int_0^{2\pi}\delta\{d_{ij}\}^T\{f_{ij}\}rd\theta + \int_0^{2\pi}\int_0^L \delta\{u\}^T\{p\}rdsd\theta = 0 \tag{19}$$

Noting the following relation

$$\int_0^{2\pi}\cos^2 n\theta d\theta = \int_0^{2\pi}\sin^2 n\theta = \pi$$

Eq. (19) can be simplified as

$$\int_0^L \delta\{\varepsilon_n\}^T\{\sigma_n\}ds + \delta\{d_{ijn}\}^T\{f_{ijn}\} + \int_0^L \delta\{u_n\}^T\{p_n\}ds = 0 \tag{20}$$

2.2. Shell Model With Uniform Circumferential Distribution of Radial Soil Spring (Shell Model-I)

Shell Model-I

Fig. 3 shows shell model-I used for the analysis. An elastic continuous thin shell

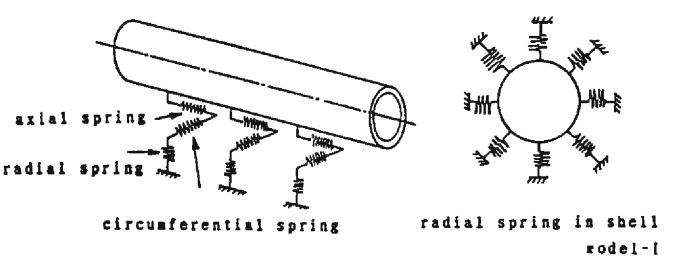

Fig. 3 Ground-pipe system of shell model-I.

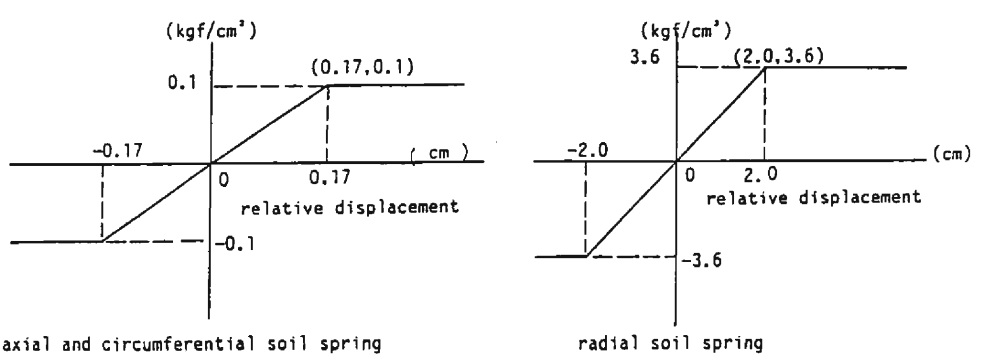

Fig. 4 Stress-relative displacement relation of soil springs in shell model-I.

is supported by the axial and circumferential shear spring and the radial spring which are distributed uniformly on the shell surface. Stress-relative displacement relations are illustrated in **Fig. 4.** Ground deformation corresponding to seismic ground motion, differential settlement, dislocation or faulting are exerted on the thin shell from the soil springs, which consequently causes the relative displacement between the pipe and the ground that is proportional to a loading or earth pressure.

By using the Hooke's law, earth pressures are written as

$$\{p\}=\begin{Bmatrix} p_x \\ p_\theta \\ p_z \\ p_\beta \end{Bmatrix}=\begin{Bmatrix} k_x(U-u) \\ k_\theta(V-v) \\ k_z(W-w) \\ 0 \end{Bmatrix} \tag{21}$$

Here p_β is added for the convenience of later use. In shell model-I, soil springs are assumed to be bilinear as shown in **Fig. 4,** then the earth pressures are simply expressed as

$$\{p_n\}=\begin{Bmatrix} p_{xn} \\ p_{\theta n} \\ p_{zn} \\ p_{\beta n} \end{Bmatrix}=\begin{Bmatrix} kx(U_n-u_n) \\ k_\theta(V_n-v_n) \\ k_z(W_n-w_n) \\ 0 \end{Bmatrix} \tag{22}$$

or

$$\{p_n\}=[k_n](\{U_n\}-\{u_n\})$$

where

$$[k_n]=\begin{bmatrix} kx & 0 & 0 & 0 \\ 0 & k_\theta & 0 & 0 \\ 0 & 0 & k_z & 0 \\ 0 & 0 & 0 & 0 \end{bmatrix} \tag{23}$$

Element Governing Eqution

By using Eqs. (22) and (11), the third term in Eq. (20) becomes

$$\begin{aligned}\int_0^L \delta\{u_n\}^T\{p_n\}\,ds &= \int_0^L \delta\{u_n\}^T[k_n](\{U_n\}-\{u_n\})\,ds \\ &= \int_0^L \delta\{d_{ijn}\}^T[N]^T[k_n](\{U_n\}-[N]\{d_{ijn}\}) \\ &= \delta\{d_{ijn}\}^T L\int_0^1 [N]^T[k_n]\{U_n\}\,d\xi \\ &\quad -\delta\{d_{ijn}\}^T L\int_0^1 [N]^T[k_n][N]\,d\xi\,\delta\{d_{ijn}\}\end{aligned} \tag{24}$$

By means of Eqs. (14) and (16), the first term in Eq. (20) leads to

$$\begin{aligned}-\int_0^L \delta\{\varepsilon_n\}^T\{\sigma_n\}\,ds &= -\int_0^L \delta\{d_{ijn}\}^T[B]^T[D][B]\{d_{ijn}\}\,ds \\ &= -\delta\{d_{ijn}\}^T L\int_0^1 [B]^T[D][B]\,d\xi\,\{d_{ijn}\}\end{aligned} \tag{25}$$

Substitute Eqs. (24) and (25) into Eq. (20) and rearrange, and it becomes

$$-L\int_0^1[B]^T[D][B]d\xi\{d_{ijn}\}+L\int_0^1[N]^T[k_n]\{U_n\}d\xi-$$
$$L\int_0^1[N]^T[k_n][N]d\xi\delta\{d_{ijn}\}+\{f_{ijn}\}=0 \tag{26}$$

If we denote $\{P_n\}$, $[K_n]$ and $[K_s]$ as

$$\{P_n\}=L\int_0^1[N]^T[k_n]\{U_n\}d\xi \tag{27}$$

$$[K_n]=L\int_0^1[B]^T[D][B]d\xi \tag{28}$$

$$[K_s]=L\int_0^1[N]^T[k_n][N]d\xi \tag{29}$$

we then obtain the governing equation of element e_{ij}.

$$\{f_{ijn}\}+\{P_n\}=([K_n]+[K_s])\{d_{ijn}\} \tag{30}$$

in which $[k_n]$ is the stiffness matrix of the pipeline, $[k_s]$ the stiffness matrix due to the soil springs, $\{f_{ijn}\}$ the nodal force vector, $\{P_n\}$ the loading vector, the calculation of which will be discussed in 2. 3.

Computation of $[K_s]$ and $[K_n]$

$[K_s]$ is computed directly. First $[N]^T[k_n][U_n]$ is calculated (see Eq. $(A-2)$ in Appendix A), then integration is carried out which leads to

$$[Ks]=\begin{pmatrix} k_z/3 & & & & & & & \\ 0 & k_z/3 & & & \text{synmetry} & & & \\ 0 & 0 & 13k_z/35 & & & & & \\ 0 & 0 & 11k_zL/210 & k_zL^2/105 & & & & \\ k_z/6 & 0 & 0 & 0 & k_z/3 & & & \\ 0 & k_\theta/6 & 0 & 0 & 0 & k_\theta/3 & & \\ 0 & 0 & 9k_z/70 & 13k_zL/420 & 0 & 0 & 13k_z/35 & \\ 0 & 0 & -13k_zL/420 & -k_zL^2/140 & 0 & 0 & -11k_zL/210 & k_zL^2/105 \end{pmatrix} \tag{31}$$

It is quite difficult to calculate $[k_n]$ by direct integration, but it can readily be evaluated by numerical integration. Due to the highest degree of polynomials of elements in $[B]$ being three, we can obtain the exact result by using the Gaussian quadrature formula of 4 degrees.

Global Relation and Boundary Condition

By assuming the governing equation (30) corresponding to all elements, we have the global relation

$$[K]\{r\}=\{P\}+\{F\} \tag{32}$$

Here $[K]$ is the global stiffness matrix which is a symmetric band matrix with a bandwidth of 15. $\{P\}$ is the global load vector, $\{F\}$, global nodal force vector, and $\{r\}$, global nodal displacement vector given by

$$\{F\}=[f_{1n},\ 0,\ 0,\ \ldots,\ 0,\ 0,\ f_{nn}] \tag{33}$$

$$\{r\}=[d_{1n},\ d_{2n},\ \ldots,\ d_{nn}] \tag{34}$$

Two boundary conditions are considered in the investigation.

(1) The free boundary condition is expressed as

$$\{f_{1n}\}=\{f_{nn}\}=0 \tag{35}$$

(2) The fixed boundary condition is given by

$$\{d_{1n}\}=\{U_{1n}\},\ \{d_{nn}\}=\{U_{nn}\} \tag{36}$$

Cholesky's method is adopted to solve the global equation. After the global nodal displacement vector is computed, strains, stresses and relative displacements of a pipe in each element can readily be evaluated.

In the case of axisymmetric loading ($n=0$), responses are also axisymmetric. Thus nodal forces Q_i, H_i, M_i, in Eq. (2) and u_i, w_i, β_i, in Eq. (4) are constant along any circumference, and their components in the circumferential direction become zero. Generalized nodal displacements and forces of arbitrary nodal line i can then be expressed as

$$\{f_{i0}\}=[Q_i(x),\ H_i(x),\ M_i(x)]^T \tag{37}$$

$$\{d_{i0}\}=[u_i(x),\ v_i(x),\ w_i(x),\ \beta_i(x)]^T \tag{38}$$

Generalized nodal displacements and forces of element e_{ij} now become

$$\{f_{ij0}\}=[Q_i(x),\ T_i(x),\ H_i(x),\ M_i(x),\ Q_j(x),\ T_j(x),\ H_j(x),\ M_j(x)]^T \tag{39}$$

$$\{d_{ij0}\}=[u_i(x),\ v_i(x),\ w_i(x),\ \beta_i(x),\ u_j(x),\ v_j(x),\ w_j(x),\ \beta_j(x)]^T \tag{40}$$

In the same procedure as that presented in 2.2, we can readily obtain the relations between displacements and nodal displacements, and those between strains and nodal displacements. Four important matrices used in Eqs. (27), (28) and (29) are:

$$\begin{pmatrix} 1-\varepsilon & 0 & 0 & \xi & 0 & 0 \\ 0 & 1-3\xi^2+2\xi^3 & L(\xi-2\xi^2+\xi^3) & 0 & 3\xi^2-2\xi^3 & -L(\xi^2-\xi^3) \\ 0 & -6(\xi-\xi^2)/L & 1-4\xi+3\xi^2 & 0 & 6(\xi-\xi^2)/L & -2\xi+3\xi^2 \end{pmatrix}\{d_{ij0}\} \tag{41}$$

$$[D_0]=\frac{Eh}{1-\nu^2}\begin{pmatrix} 1 & \nu & 0 \\ \nu & 1 & 0 \\ 0 & 0 & h^2/12 \end{pmatrix} \tag{42}$$

$$[k_0]=\begin{pmatrix} k_x & 0 & 0 \\ 0 & k_z & 0 \\ 0 & 0 & 0 \end{pmatrix} \tag{43}$$

and $[B_0]$ is expressed in Eq. $(A-3)$ (see appendix A)

$[K_e]$ can also be calculated directly from

$$[K_e]=\begin{pmatrix} k_x/3 & & & & \text{Symmetric} & \\ 0 & 13k_z/35 & & & & \\ 0 & 11k_zL/210 & k_zL^2/105 & & & \\ k_x/6 & 0 & 0 & k_x/3 & & \\ 0 & 9k_z/70 & 13k_zL/420 & 0 & 13k_z/35 & \\ 0 & -13k_zL/420 & -k_zL^2/140 & 0 & -11k_zL/210 & k_zL^2/105 \end{pmatrix} \tag{44}$$

$[K_0]$ is computed by the Gaussian quadrature and $\{P_0\}$ corresponding to several kinds of load inputs is evaluated in 2.3. The global relation and boundary condition are of the same form as those in 2.2.

2.3. Ground Displaaement and Loading Vectors of Shell Model-I : Loading Vectors of Seismic Ground Motion

Loading Vectors of Seismic Waves

Assume that the seismic wave can be treated as a sinusoidal function of time t and axial coordinate x propagating in x-z plane with an incident angle α with respect to the axis of the pipeline (x-axis) as shown in **Fig. 5.** Then the displacement components

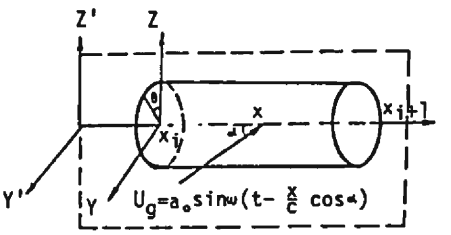

Fig. 5 Seismic wave loading.

in x, θ, z directions are, respectively,

Longitudinal wave:

$$\{U\}=\begin{Bmatrix}U\\V\\W\end{Bmatrix}=\begin{Bmatrix}a_0\cos\alpha\ \sin\omega(t-x\cos\alpha/c)\\-a_0\sin\alpha\ \sin\omega(t-x\cos\alpha/c)\ \sin\theta\\a_0\sin\alpha\ \sin\omega(t-x\cos\alpha/c)\ \cos\theta\end{Bmatrix} \tag{45}$$

Transverse wave:

$$\{U\}=\begin{Bmatrix}U\\V\\W\end{Bmatrix}=\begin{Bmatrix}-a_0\sin\alpha\ \sin\omega(t-x\cos\alpha/c)\\-a_0\cos\alpha\ \sin\omega(t-x\cos\alpha/c)\ \sin\theta\\a_0\cos\alpha\ \sin\omega(t-x\cos\alpha/c)\ \cos\theta\end{Bmatrix} \tag{46}$$

They can be easily separated into two parts. For a longitudinal wave,

$n=1$:

$$\{U_1\}=\begin{Bmatrix}U\\V\\W\\\beta\end{Bmatrix}=\begin{Bmatrix}0\\-a_0\sin\alpha\ \sin\omega(t-x\cos\alpha/c)\\a_0\sin\alpha\ \sin\omega(t-x\cos\alpha/c)\\0\end{Bmatrix} \tag{47}$$

$n=0$:

$$\{U_0\}=\begin{Bmatrix}U\\W\\\beta\end{Bmatrix}=\begin{Bmatrix}a_0\cos\alpha\ \sin\omega(t-x\cos\alpha/c)\\0\\0\end{Bmatrix} \tag{48}$$

For a transverse wave,

$n=1$:

$$\{U_1\}=\begin{Bmatrix}U\\V\\W\\\beta\end{Bmatrix}=\begin{Bmatrix}0\\-a_0\cos\alpha\sin\omega(t-x\cos\alpha/c)\\a_0\cos\alpha\sin\omega(t-x\cos\alpha/c)\\0\end{Bmatrix}. \tag{49}$$

$n=0$:

$$\{U_0\}=\begin{Bmatrix}U\\W\\\beta\end{Bmatrix}=\begin{Bmatrix}-a_0\cos\alpha\sin\omega(t-x\cos\alpha/c)\\0\\0\end{Bmatrix} \tag{50}$$

In order to calculate loading vector $\{P_n\}$, by means of Eq. (11), $[N]^T[k_n][U_n]$ is calculated first;

$$[N]^T[k_n]\{U_n\}=\begin{Bmatrix}k_xU_n(1-\xi)\\k_\theta V_n(1-\xi)\\k_zW_n(1-3\xi^2+2\xi^3)\\k_zW_nL(\xi-2\xi^2+\xi^3)\\k_xU_n\xi\\k_\theta V_n\xi\\k_zW_n(3\xi^2-2\xi^3)\\k_zW_nL(\xi^2-\xi^3)\end{Bmatrix} \tag{51}$$

Substituting Eq. (51) into Eq. (38) and integrating, we obtain the loading vector:

$$\{P_1\}=[P_1,\ P_2,\ P_3,\ P_4,\ P_5,\ P_6,\ P_7,\ P_8]^T \tag{52}$$

For a longitudinal wave:

$$\left.\begin{aligned}P_1&=0\\P_2&=-a_0\ k_\theta\sin\alpha\ f_1\\P_3&=a_0\ k_z\sin\alpha\ f_3\\P_4&=a_0\ k_z\ L\sin\alpha\ f_4\\P_5&=0\\P_6&=-a_0\ k_\theta\sin\alpha\ f_6\\P_7&=a_0\ k_z\sin\alpha\ f_7\\P_8&=-a_0\ k_z\ L\sin\alpha\ f_8\end{aligned}\right\} \tag{53}$$

For a transevers wave:

$$\left.\begin{aligned}P_1&=0\\P_2&=-a_0\ k_\theta\cos\alpha\ f_1\\P_3&=a_0\ k_z\cos\alpha\ f_3\\P_4&=a_0\ k_z\ L\cos\alpha\ f_4\\P_5&=0\\P_6&=-a_0\ k_\theta\cos\alpha\ f_6\\P_7&=a_0\ k_z\cos\alpha\ f_7\\P_8&=-a_0\ k_z\ L\cos\alpha\ f_8\end{aligned}\right\} \tag{54}$$

where f_i, $i=1, 3, 4, 6, 7, 8$ are shown in Eq. (A−4) (see appendix A).

Loading vectors of the axisymmetric load $\{P_0\}$ are derived in the same way. They can be expressed as

$$\{P_0\}=[P_1,\ P_2,\ P_3,\ P_4,\ P_5,\ P_6]^T \tag{55}$$

For a longitudinal wave:

$$\left.\begin{aligned} P_1&=k_x a_0 f_1 \cos\alpha \\ P_4&=k_x a_0 f_3 \cos\alpha \\ P_2&=P_3=P_5=P_6=0 \end{aligned}\right\} \tag{56}$$

For a transverse wave:

$$\left.\begin{aligned} P_1&=-k_x a_0 f_1 \sin\alpha \\ P_4&=-k_x a_0 f_3 \sin\alpha \\ P_2&=P_3=P_5=P_6=0 \end{aligned}\right\} \tag{57}$$

Loading Vectors of Dislocation and Differential Settlement

Assume that a ground dislocation takes place in such a way that the right-hand part slips upward with an inclination angle α, and the left-hand part remains unmoved. For the requirement of the continuity of displacements of the ground, the displacements in the connected element e_{AB} is supposed to be linear (see **Fig. 6**). Then the ground displacement vectors are represented as follows. In the connecting element e_{AB},

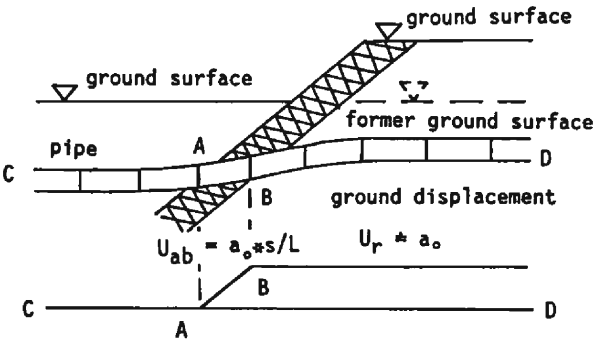

Fig. 6 Ground displacement of dislocation.

$$\{U_{AB}\}=\begin{Bmatrix} U \\ V \\ W \end{Bmatrix}=\begin{Bmatrix} sa_0\cos\alpha/L \\ sa_0\sin\alpha\sin\theta/L \\ sa_0\sin\alpha\cos\theta/L \end{Bmatrix} \tag{58}$$

In the right part BD

$$\{U\}_r=\begin{Bmatrix} U \\ V \\ W \end{Bmatrix}=\begin{Bmatrix} a_0\cos\alpha \\ a_0\sin\alpha\sin\theta \\ a_0\sin\alpha\cos\theta \end{Bmatrix} \tag{59}$$

In the left part

$$\{U\}_L=0 \tag{60}$$

With the same procedure as used in the deduction of Eqs. (53), (54), (56) and (57), we obtain the corresponding loading vectors. For $n=1$, in the connecting element,

$$\{P_1\}=L\begin{Bmatrix}0\\ k\ a_0\sin\alpha/6\\ 3k_z a_0\sin\alpha/20\\ k_z La_0\sin\alpha/30\\ 0\\ k\ a_0\sin\alpha/3\\ 7k_z a_0\sin\alpha/20\\ -k_z La_0\sin\alpha/20\end{Bmatrix} \tag{61}$$

In the right part BD,

$$\{P_1\}=\frac{L}{2}\begin{Bmatrix}0\\ k\ a_0\sin\alpha\\ 3k_z a_0\sin\alpha\\ k_z La_0\sin\alpha/6\\ 0\\ k\ a_0\sin\alpha\\ 7k_z a_0\sin\alpha\\ -k_z La_0\sin\alpha/6\end{Bmatrix} \tag{62}$$

For $n=0$, in the connecting element,

$$\{P_0\}=\begin{Bmatrix}k_z La_0\cos\alpha/6\\ 0\\ 0\\ k_z La_0\cos\alpha/3\\ 0\\ 0\end{Bmatrix} \tag{63}$$

In the right part,

$$\{P_0\}=\begin{Bmatrix}k_z La_0\cos\alpha\\ 0\\ 0\\ k_z La_0\cos\alpha/2\\ 0\\ 0\end{Bmatrix} \tag{64}$$

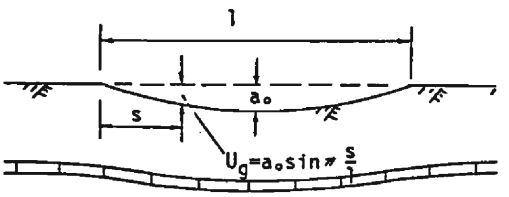

Fig. 7 Differential settlement loading.

Assume that a ground differential settlement occurs in the shape of a half length of isnusoidal function (see **Fig. 7**). Thus, the loading vector in AB is the same as that in Eqs. (53), (54), (56) and (57) and becomes zero in other areas.

2.4. Shell Model With Nonuniform Circumferential Distribution of Radial Soil Spring (Shell Model-II) and the Corresponding Loading Vector

Shell Model-II

Radial earth pressure corresponding to the assumption of the stress-relative displacement relation employed in shell model-I is shown in **Fig. 8.** However, there exists no or very small pull between pipes and ground. Thus, radial earth pressure is distributed as that shown in **Fig. 9** provided the earth pressure at rest is neglected. To consider this distribution, radial springs were assumed to be nonsymmetrically distributeed (see **Fig. 10**), but axial and circumferential springs were kept unchanged as in model I. The pipe-ground interaction system idealized as a thin shell supported by these three kinds of springs will be called shell model-II for the convenience of description. The corresponding radial stress-relative displacement relation is illustrated in **Fig. 11.** Here Eq. (21) becomes

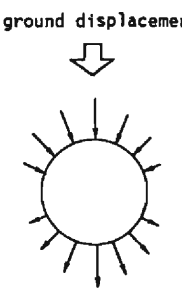

Fig. 8 Earth pressure corresponding to shell model-I.

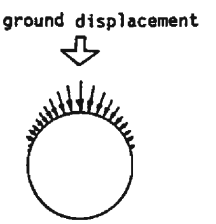

Fig. 9 Realistic radial earth pressure.

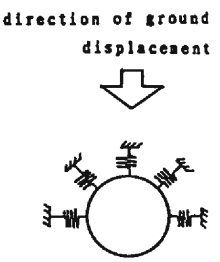

Fig. 10 Ristribution of radial spring corresponding to shell model-II.

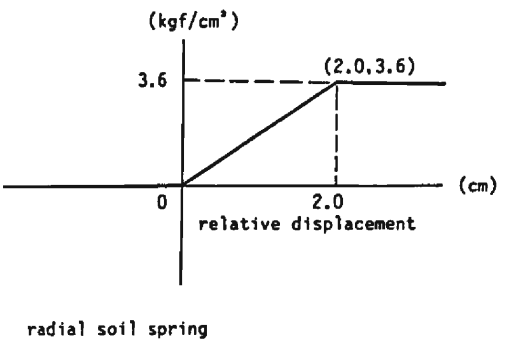

Fig. 11 Stress-relative displacement relation of radial spring in shell model-II.

$$\{p\}=\begin{Bmatrix} p_x \\ p_\theta \\ p_z \\ p_\beta \end{Bmatrix}=\begin{Bmatrix} k_x(U-u) \\ k_\theta(V-v) \\ k_z'(W-w) \\ 0 \end{Bmatrix} \tag{65}$$

where

$$k_z'=\begin{cases} 0 & W-w>0 \\ k_z & W-w<0 \end{cases} \tag{66}$$

Consider the ground movement downwards first [$\mathrm{Sin}\,\omega(t-x\,\mathrm{Cos}\,\alpha/c)<0$], k_z being rewritten as

$$k_z'=\begin{cases} 0 & \pi/2<\theta<3\pi/2 \\ k_z & -\pi/2<\theta<\pi/2 \end{cases} \tag{67}$$

If the relative ground movement is a cosine distribution along the circumference, i, e.,

$$W=W_a(x)\cos\theta \tag{68}$$

then the radial displacement of the pipeline may also be assumed to have the same distribution (This is obviously not true due to the deformation of the cross section, the difference being less significant in the description of each pressure.) given by

$$W=W_a(x)\cos\theta \tag{69}$$

Thus the radial earth pressure can be rewritten as

$$p_z=[W_a(x)-w_a(x)]k_z'\cos\theta \tag{70}$$

where

$$k_z'\cos\theta=\begin{cases} 0 & \pi/2<\theta<3\pi/2 \\ k_z\cos\theta & -\pi/2<\theta<\pi/2 \end{cases} \tag{71}$$

which can readily be approximated by a finite Fourier series as

$$K_z'\cos\theta=k_z\{1/\pi+\cos\theta/2+(-1)^{k+1}2/\pi\sum\cos 2k\theta/(4k^2+1)\} \tag{72}$$

Consider the harmonic number merely up to $2k=10$. We can obtain a good approximation given by

$$\begin{aligned} k_z'\cos\theta=&k_z\{1/\pi+\cos\theta/2+2\cos 2\theta/(3\pi)-2\cos 4\theta/(15\pi) \\ &+2\cos 6\theta/(35\pi)-2\cos 8\theta/(63\pi)+2\cos 10\theta/(99\pi)\} \\ =&k_zC_0+k_zC_1+k_zC_2+k_zC_4+k_zC_6+k_zC_8+k_zC_{10} \end{aligned} \tag{73}$$

where

$$\left.\begin{aligned} &C_0=1/\pi \quad C_1=1/2 \quad C_2=2/(3\pi) \quad C_4=-2/(15\pi) \\ &C_6=2/(35\pi) \quad C_8=-2/(63\pi) \quad C_{10}=2/(99\pi) \end{aligned}\right\} \tag{74}$$

Substituting Eq. (73) into Eq. (70) leads to

$$\begin{aligned} p_z=&(p_{z0}+p_{z1}+p_{z2}+p_{z4}+p_{z6}+p_{z8}+p_{z10}) \\ =&\{[W_0(x)-w_0(x)]+[W_1(x)-w_1(x)] \\ &+[W_2(x)-w_2(x)]+[W_4(x)-w_4(x)]+[W_6(x)-w_6(x)] \\ &+[W_8(x)-w_8(x)]+[W_{10}(x)-w_{10}(x)]\} \end{aligned} \tag{75}$$

in which

$$\begin{cases} W_0(x) = C_0 W_a(x) \\ W_1(x) = C_1 W_a(x) \\ W_2(x) = C_2 W_a(x) \\ W_4(x) = C_4 W_a(x) \\ W_6(x) = C_6 W_a(x) \\ W_8(x) = C_8 W_a(x) \\ W_{10}(x) = C_{10} W_a(x) \end{cases} \tag{76}$$

$W_a(x)$, which corresponds to p_{zn}, is called the apparent radial ground displacement, and $W_n(x)$ is the corresponding radial displacement of the pipeline.

If the ground moves upwards $[\mathrm{Sin}\,\omega(t - x\,\mathrm{Cos}\,\alpha/c) > 0]$, we can derive the same expression as Eq. (75) and (76). However, here C_n is

$$\begin{cases} C_0 = -1/\pi \quad C_1 = 1/2 \quad C_2 = -2/(3\pi) \quad C_4 = 2/(15\pi) \\ C_6 = -2/(35\pi) \quad C_8 = 2/(63\pi) \quad C_{10} = -2/(99\pi) \end{cases} \tag{77}$$

From the above observation, we know that in order to take the actual earth pressure into consideration, it is merely necessary to change the radial displacement in Eq. (45) into its apparent displacement, then following the procedure pressented in **2.2**, we can arrive at the element governing equation (30). Matrix $[K_n]$, $[K_s]$ and column vector $\{f_{ijn}\}$ are completely the same. However, loading vectors $\{P_n\}$, corresponding to various kinds of loadings, are changed due to the change of expression of radial displacement. We will discuss them in detail in the following.

Loading Vectors of Longitudinal Waves

The apparent ground displacements excited by a longitudinal wave are

$$\{U\} = \begin{Bmatrix} \mathrm{U} \\ V \\ W \end{Bmatrix} = \begin{Bmatrix} a_0 \cos\alpha \sin\omega(t - x\cos\alpha/c) \\ -a_0 \sin\alpha \sin\omega(t - x\cos\alpha/c) \\ W_0(x) + W_1(x)\cos\theta + W_2(x)\cos 2\theta + W_4(x)\cos 4\theta \\ + W_6(x)\cos 6\theta + W_8(x)\cos 8\theta + W_{10}(x)\cos 10\theta \end{Bmatrix} \tag{78}$$

here $W_a(x)$ is

$$W_a(x) = a_0\,\mathrm{Sin}\,\alpha\,\mathrm{Sin}\,\omega(t - x\,\mathrm{Cos}\,\alpha/c) \tag{79}$$

Thus

$$\begin{cases} W_0(x) = C_0 a_0 \sin\alpha \sin\omega(t - x\cos\alpha/c) \\ W_1(x) = C_1 a_0 \sin\alpha \sin\omega(t - x\cos\alpha/c) \\ W_2(x) = C_2 a_0 \sin\alpha \sin\omega(t - x\cos\alpha/c) \\ W_4(x) = C_4 a_0 \sin\alpha \sin\omega(t - x\cos\alpha/c) \\ W_6(x) = C_6 a_0 \sin\alpha \sin\omega(t - x\cos\alpha/c) \\ W_8(x) = C_8 a_0 \sin\alpha \sin\omega(t - x\cos\alpha/c) \\ W_{10}(x) = C_{10} a_0 \sin\alpha \sin\omega(t - x\cos\alpha/c) \end{cases} \tag{80}$$

Apparently the ground displacement can be separated into seven parts. By means of

Eq. (27), the loading vectors of a longitudinal wave are:

$n=0$

$$\{P_0\}=[P_1,\ P_2,\ P_3,\ P_4,\ P_5,\ P_6]^T \tag{81}$$

where

$$\begin{cases} P_1=k_x a_0 f_2 \cos\alpha & P_2=W_0(x) f_3 \quad P_3=W_0(x) L f_4 \\ P_4=k_x a_0 f_6 \cos\alpha & P_5=W_0(x) f_7 \quad P_6=-W_0(x) L f_8 \end{cases} \tag{82}$$

in which f is shown in Eq. $(A-4)$ (see appendix A).

$n=1$

$$\{P_1\}=[P_1,\ P_2,\ P_3,\ P_4,\ P_5,\ P_6,\ P_7,\ P_8]^T \tag{83}$$

where

$$\begin{cases} P_1=0 \\ P_2=-a_0 k_0 f_2 \sin\alpha \\ P_3=W_1(x) f_3 \\ P_4=W_1(x) L f_4 \\ P_5=0 \\ P_6=-a_0 k_0 f_6 \sin\alpha \\ P_7=W_1(x) f_7 \\ P_8=-W_1(x) f_8 \end{cases} \tag{84}$$

$n=2,\ 4,\ 6,\ 8,\ 10$

$$\begin{cases} P_1=0 \\ P_2=0 \\ P_3=W_n(x) f_3 \\ P_4=W_n(x) L f_4 \\ P_5=0 \\ P_6=0 \\ P_7=W_n(x) f_7 \\ P_8=-W_n(x) f_8 \end{cases} \tag{85}$$

In the same procedure, we could obtain the loading vectors of a transverse wave, ground dislocation and differential settlement. Nevertheless, we hcve expressed them in Eq. (A-5)$\sim$(A-15) (see Appendix A).

3. Discussion of Calculation Results

3.1. Comparison of Three Kinds of Models

Fig. 12 shows the response values of a pipe disturbed by a longitudinal wave with a displacement amplitude of 5 cm and an incident angle of 45 degree. The axial displacement and stress of the pipe indicated by three models are almost exactly the same. A maximum axial stress of 670 kgf/cm^2 occurs. Shell model-I and shell model-II illustrate that the circumferential stress, which can not be calculated from the beam model, is approximately 1/3 of the axial one.

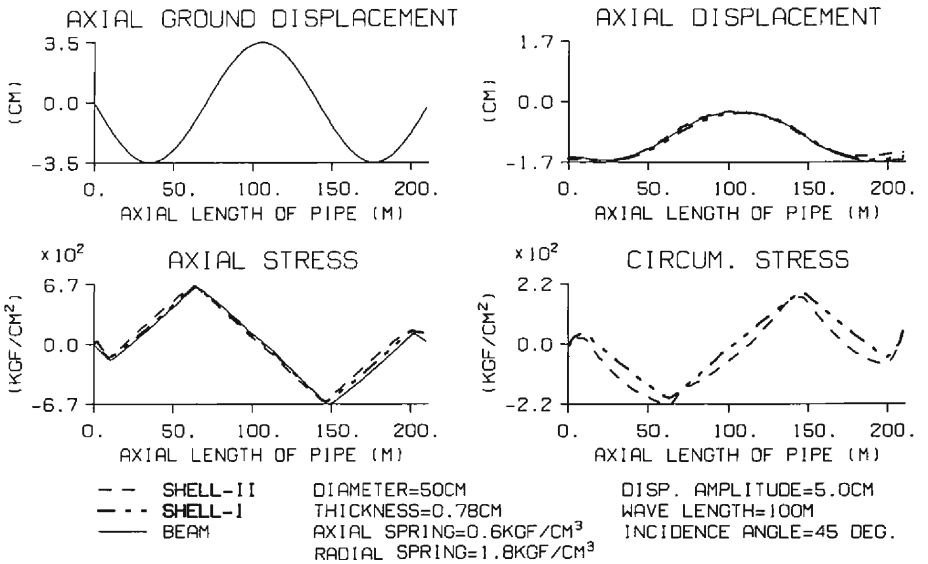

Fig. 12 Response values of a pipe subjected to longitudinal wave.

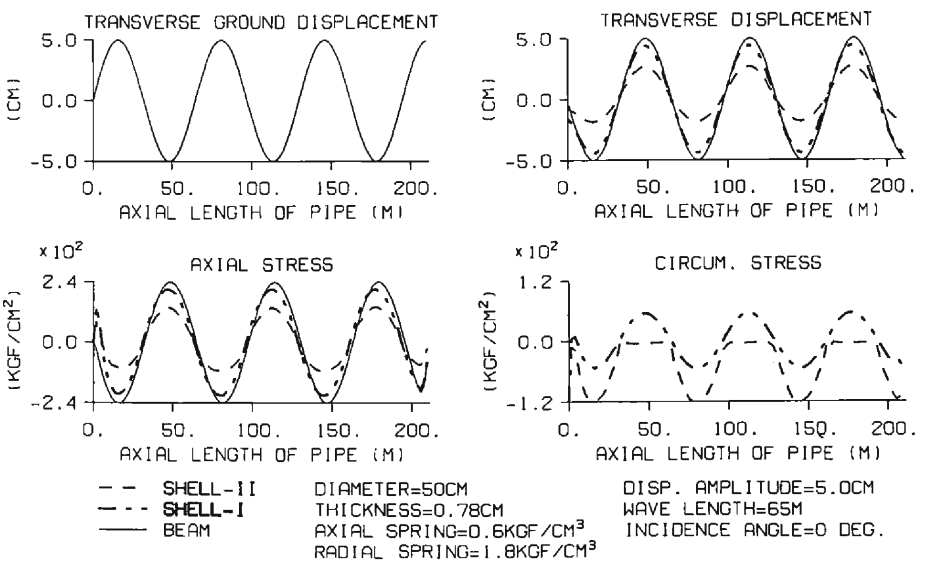

Fig. 13 Response values of a pipe subjected to transverse wave.

Fig. 13 illustrates the results of a pipe excited by an axially incident transverse wave with a displacement amplitude of 5 cm. The axial stress and transverse displacement of the pipe obtained by the beam model and shell model-I are very close. However, shell model-II gives much smaller results. Shell model-II shows that larger circumferential stress occurred than that obtained by shell model-I. These differences are considered to be from the influence of earth pressure. The beam model and shell model-I do not

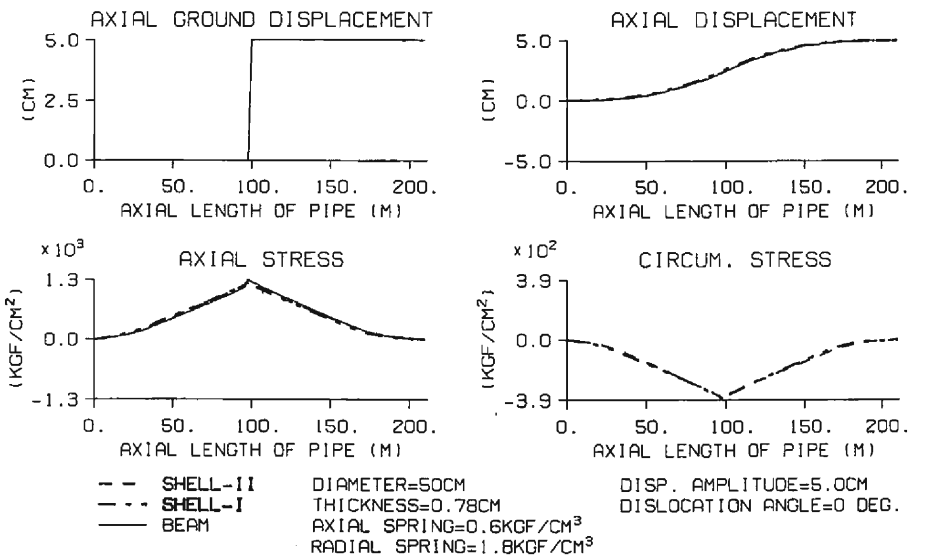

Fig. 14 Calculation results of a pipe under horizontal dislocation.

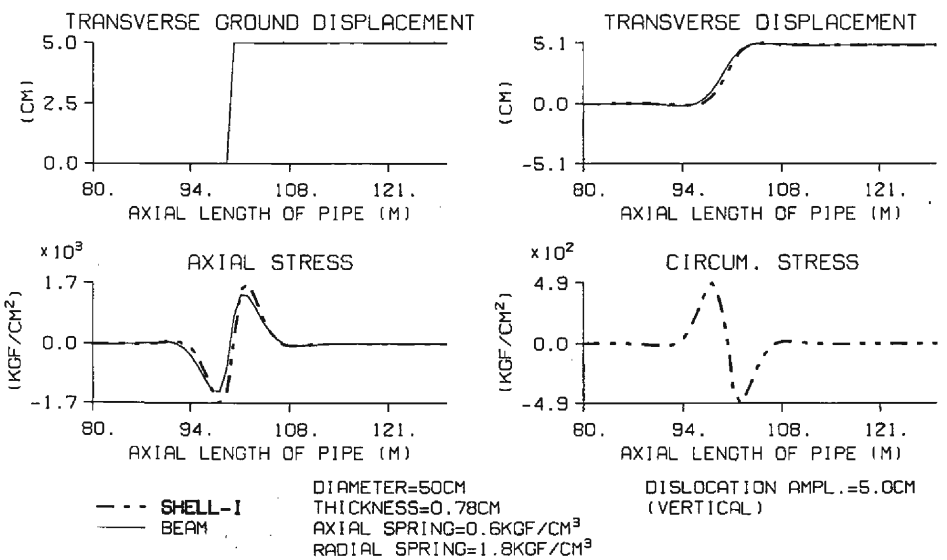

Fig. 15 Calculation results of a pipe under vertical dislocation.

take the real distribution of earth pressure into consideration. We will discuss this point in more detail later.

In **Fig. 14,** the results of a pipe subjected to a 5 cm horizontal dislocation are plotted. All the responses given by the three models are almost exactly the same. It is obvious that a large axial stress of 1300 kgf/cm² takes place in this case.

Fig. 15 presents the results of a pipeline subjected to a vertical ground dislocation.

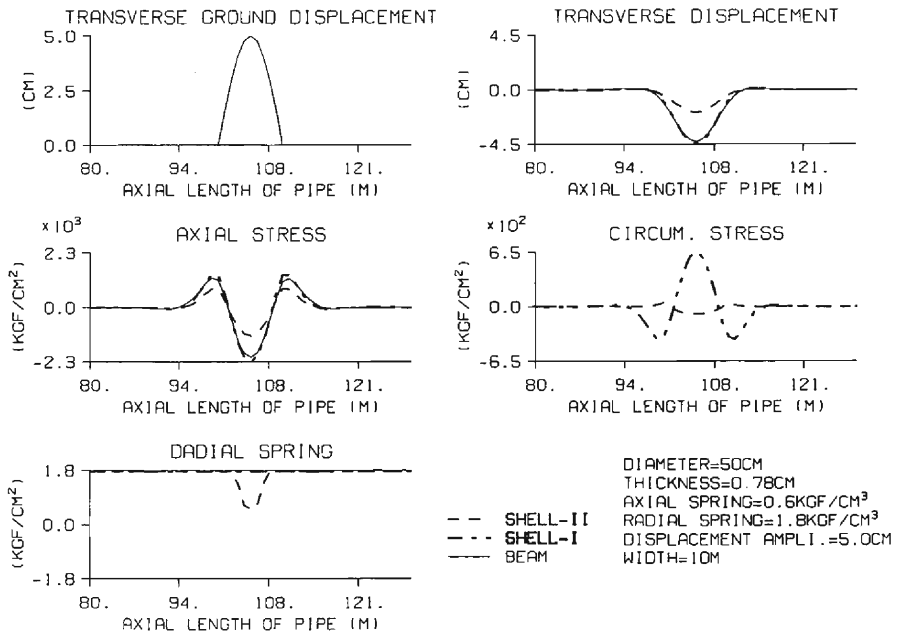

Fig. 16 Calculation results of a pipe under differential settlement.

Both the beam model and shell model-I show approximately same axial stress of 1700 kgf/cm². Nevertheless, this may be overestimated due to the fact that earth pressure has not been considered.

Fig. 16 shows the results for a pipe under a differential settlement with maximum value of 5 cm. The response values obtained from the beam model and shell model-I are also quite larger than those calculated from shell model-II. But even shell model-II indicates that 1300 kgf/cm² axial stress occurred. This is much greater than those generated by a longitudinal wave or a transverse wave. Moreover, when the displacement amplitude increases, the axial stress increases proportionally.

From the above observation, we can conclude that the beam model, shell model-I and shell model-II are all suitable for the calculation of axial stress under the ground deformation in the axial direction, which is usually the most significant stress in the case of axial ground deformation loadings such as an axial incident longitudinal wave and horizontal dislocation. However, the beam model and shell model-I over estimates the axial stress in the case of transverse ground deformation loading such as an axial incident *SV* wave and differential settlement. Differential settlement can generate much greater stresses than other kinds of loadigs. This may explain to some extent why the damage in soft ground areas is severer.

3.2. Results for Transverse Ground Deformation Loadings

As mentioned in the former section, the beam model and shell model-I always give approximately the same axial stress in all kinds of loadigns considered in this paper. So we will discuss the results solely by means of shell model-I and shell model-II.

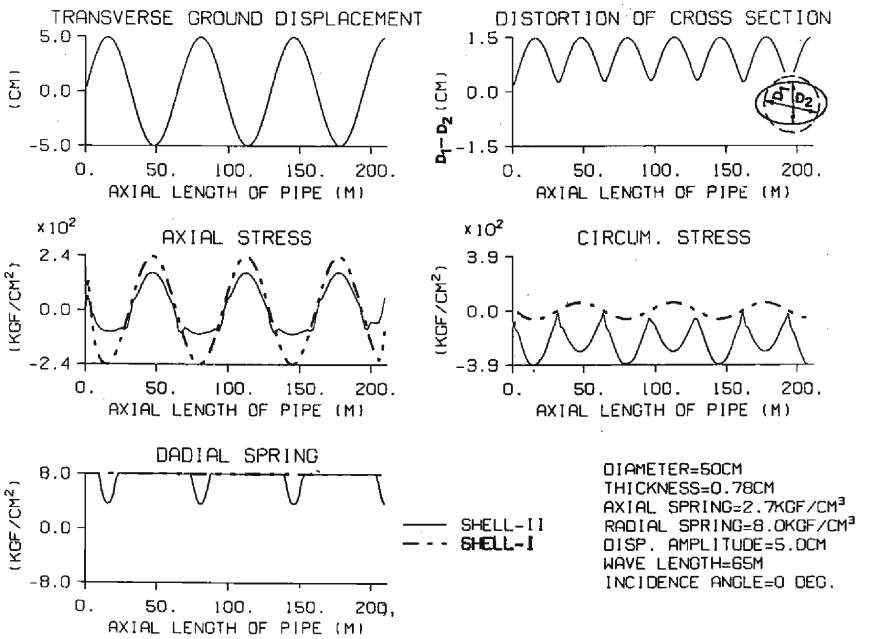

Fig. 17 Response values of a pipe embedded in stiff ground excited by transverse wave.

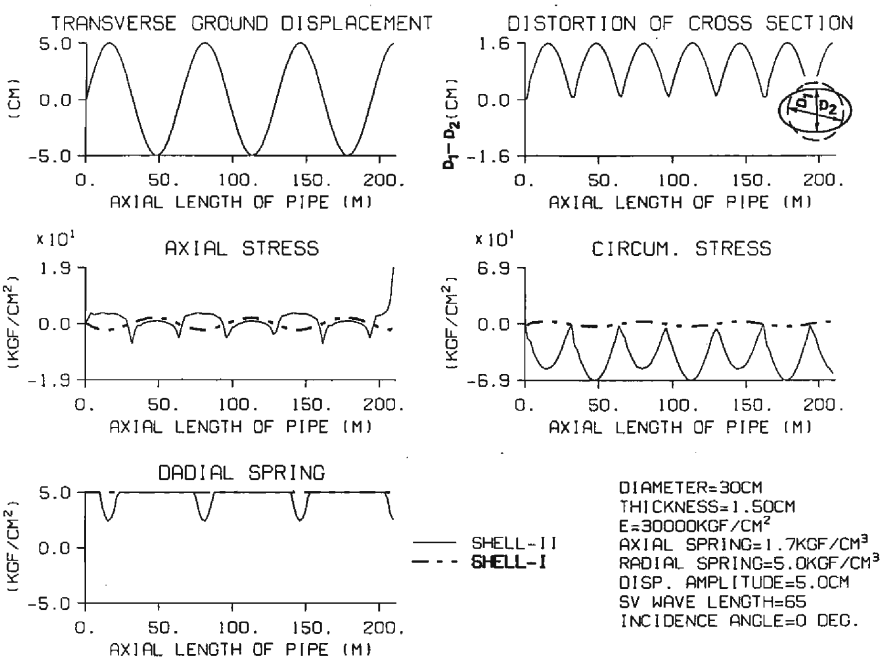

Fig. 18 Response values of a PVC pipe embedded in stiff ground excited by transverse wave.

Results for Transverse Wave Loading

Fig. 17 shows the responses of a pipe embedded in stiff ground subjected to an axial incident transverse wave with an amplitude of 5 cm and wave length of 65 m. Shell model-II shows that 390 kgf/cm^2 circumferential stress occurred, which is greater than the axial stress. Maximum distortion of 1.5 cm was obtained from shell model-II which was not the case with shell model-I. Shell model-I gives a larger axial stress but smaller circumferential stress than those calculated by shell model-II. Shell model-II also showed that plasticity of radial spring takes place in some areas, while shell model-I does not indicate this phenomenon.

In **Fig. 18,** the results of a PVC pipe embedded in stiff ground excited by a transverse wave with an amplitude of 5 cm are plotted.

A circumferential stress of 69 kgf/cm^2 was obtained from shell model-II. Shell model-II also showed that distortion of the pipe section and plasticity took place.

The reason that the two models give different results is shown in **Fig. 19.** In shell model-I, earth pressure corresponding to transverse wave loading was considered to be distributed as that in (B). However, a realistic earth pressure was considered as that in (C) (i. e., there exists no tension between pipes and ground). This distribution is taken into

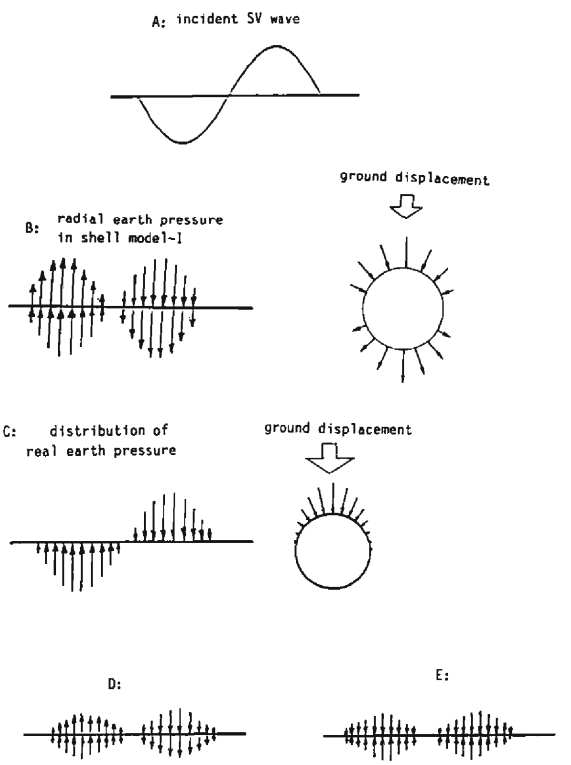

Fig. 19 Comparison of radial earth pressure in shell model-I and shell model-II.

consideration in shell model-II. The actual earth pressure can be separated into two parts, that is the symmetric part and the antisymmetric part (see (D) and (E)). The antisymmetric part is distributed in the same way as that in shell model-I except that the amplitude is only half as large. Thus the difference is caused by the symmetric part. The symmetric part not only generates smaller stresses than the antisymmetric one, but also causes plasticity to occur earlier as a common case. Thus axial stress obtained from shell model-I may be two times larger than the that calculated from shell model-II. Nevertheless, when the ground is stiff or the pipe is thin, the symmetric part can cause large distortion of the pipe cross section which can cause the circumferential stress to become more important than the axial stress.

Results for Differential Settlement Loading

Table. 1 summarizes the results (circumferential stresses are much smaller than the axial one, so they are not shown in the table) of five kinds of pipes under differential settlement with a maximum displacement of 10 cm, widths of 5, 10 and 20 cm. The radial spring constant is 1.8 kgf/cm^3 and the critical radial relative displacement (i.e. the relative displacement at which point plasticity occurs) is 4 cm which correspond to a common ground condition. It is obvious that axial stress decreases as the width of differential settlement increases, provided maximum differential settlement is the same. When the width is large, axial stress increases as the diameters of the pipe increase.

Table. 1 Axial stress of pipes subjected to differential settlement

width of dif. set, (m)	diameter (cm)	thicknvss (cm)	axial stress (kgf/cm^2) model-II	axial stress (kgf/cm^2) model-I	σ shell-II / σ shell-I
5	10	0.42	1349	3685	0.37
	32	0.69	2271	6373	0.37
	50	0.84	2206	6021	0.37
	70	0.90	2317	5598	0.41
	100	1.10	2100	4416	0.48
10	10	0.42	883	1656	0.53
	32	0.69	1387	3373	0.41
	50	0.84	1759	4432	0.40
	70	0.90	2006	5013	0.40
	100	1.10	2124	5026	0.42
20	10	0.42	498	881	0.57
	32	0.69	826	1518	0.54
	50	0.84	977	1755	0.56
	70	0.90	1132	1970	0.57
	100	1.10	1300	2668	0.49

max. dif. settlement=10 cm
radial spring constant=1.8 kgf/cm^3
critical radial relative displacement=4.0 cm

However, a maximum axial stress of 2271 kgf/cm² occurred in the pipe with a diameter of 32 cm when the width of differential settlement is 5 m.

Table. 2 shows the results of there kinds of pipes embedded in different kinds of ground subjected to differential settlement with widths of 10 m and maximum differential settlements of 10 cm. It is apparent that axial stresses increase as the ground changes from soft to stiff (i. e., the increase of spring constant or critical relative displacement). The ratio of axial stress obtained from shell model-II to that computed from shell model-II increase as the critical relative displacement increases provided the radial spring constant keeps the same. In the case of small diameter, this ratio also increases when the radial

Table. 2 Axial stress and stress ratio of pipes subjected to differential settlement under different ground conditions

diameter (cm)	Thickness (cm)	radial spring constant (kgf/cm³)	critical relative displacement (cm)	axial stress (kgf/cm²) model-II	model-I	$\frac{\sigma \text{ shell-II}}{\sigma \text{ shell-I}}$
10	0.42	0.3	2.0	256	887	0.292
	0.42	0.3	4.0	358	887	0.404
	0.42	0.3	10.0	461	887	0.520
	0.42	1.8	2.0	732	1656	0.442
	0.42	1.8	4.0	883	1656	0.533
	0.42	1.8	10.0	906	1656	0.547
	0.42	6.0	2.0	1147	2377	0.483
	0.42	6.0	4.0	1266	2377	0.533
	0.42	6.0	10.0	1265	2377	0.532
50	0.84	0.3	2.0	556	2221	0.251
	0.84	0.3	4.0	862	2452	0.352
	0.84	0.3	10.0	1226	2393	0.512
	0.84	1.8	2.0	1207	4432	0.272
	0.84	1.8	4.0	1759	4432	0.397
	0.84	1.8	10.0	2302	4432	0.52
	0.84	6.0	2.0	1855	5289	0.351
	0.84	6.0	4.0	2322	5289	0.441
	0.84	6.0	10.0	2711	5289	0.513
100	1.10	0.3	2.0	519	1536	0.338
	1.10	0.3	4.0	798	2117	0.377
	1.10	0.3	10.0	1459	2384	0.612
	1.10	1.8	2.0	1584	5383	0.294
	1.10	1.8	4.0	2124	5026	0.423
	1.10	1.8	10.0	3208	5441	0.590
	1.10	6.0	2.0	2251	7518	0.299
	1.10	6.0	4.0	3316	7518	0.441
	1.10	6.0	10.0	4320	7905	0.546

width of dif. settlement=10 cm
max. dif. settlement=10 cm

spring constant increases. This means that in the case of soft ground, stresses estimated by means of shell mode-I are much more different than the actual one. When there is no plasticity taken place, the ratio changes from 0.5 to 0.65.

If we could describe this ratio with a formula, it would be very useful and convenient because we could estimate realistic axial stress by means of the conventional beam model with the help of this formula Eq. (86) is presented for this purpose based on a large amount of calculation results.

$$\frac{\sigma \text{ shell-II}}{\sigma \text{ shell-I}} = C - \alpha\left(\frac{a_0}{U_c} - 1\right)^{\beta} \tag{86}$$

in which a_0 is the maximum differential settlement, u_c the critical relative displacement, c, α and β are parameters which change with radial spring constant and width of differential settlement.

for width = 5 m.

$$k_3 = 0.3 \text{ kgf/cm}^3 \quad \left.\begin{aligned} C &= 0.547 - 0.414D + 1.045D^2 - 0.522D^3 \\ \alpha &= 0.187 - 0.122D + 0.252D^2 - 0.172D^3 \\ \beta &= 0.418 - 1.464D + 1.693D^2 - 0.545D^3 \end{aligned}\right\} \tag{87}$$

$$k_3 = 1.8 \text{ kgf/cm}^3 \quad \left.\begin{aligned} C &= 0.563 - 0.511D + 1.423D^2 - 0.788D^3 \\ \alpha &= 0.147 - 0.316D + 1.97D^2 - 0.780D^3 \\ \beta &= 0.523 + 0.902D - 3.951D^2 + 3.042D^3 \end{aligned}\right\} \tag{88}$$

$$k_3 = 6.0 \text{ kgf/2m}^3 \quad \left.\begin{aligned} C &= 0.593 - 0.595D + 1.448D^2 - 0.784D^3 \\ \alpha &= 0.0364 + 0.678D - 0.879D^2 + 0.409D^3 \\ \beta &= 1.931\ 6.537D + 9.478D^2 - 4.554D^3 \end{aligned}\right\} \tag{89}$$

for width = 10 m,

$$R_3 = 0.3 \text{ kgf/cm}^3 \quad \left.\begin{aligned} C &= 0.532 - 0.141D + 0.180D^3 + 0.040D^2 \\ \alpha &= 0.0667 + 0.245D - 0.374D^3 + 0.284D^2 \\ \beta &= 0.709 - 0.127D - 0.756D^3 + 0.341D^2 \end{aligned}\right\} \tag{90}$$

$$R_3 = 1.8 \text{ kgf/cm}^3 \quad \left.\begin{aligned} C &= 0.590 - 0.519D + 0.947D^2 - 0.422D^3 \\ \alpha &= 0.0169 - 0.0045D + 0.441D^2 - 0.318D^3 \\ \beta &= 1.785 - 3.684D + 3.845D^2 - 1.345D^3 \end{aligned}\right\} \tag{91}$$

$$R_3 = 6.0 \text{ kgf/cm}^3 \quad \left.\begin{aligned} C &= 0.598 - 0.490D + 0.841D^2 - 0.404D^3 \\ \alpha &= 0.0133 - 0.0064D + 0.264D^2 - 0.198D^3 \\ \beta &= 1.379 - 2.707D + 4.214D^2 - 2.014D^3 \end{aligned}\right\} \tag{92}$$

for width = 20 m,

$$R_3 = 0.3 \text{ kgf/cm}^3 \quad \left.\begin{aligned} C &= 0.575 - 0.209D + 0.177D^2 - 0.0097D^3 \\ \alpha &= 0.0061 + 0.225D - 0.256D^2 + 0.142D^3 \\ \beta &= 1.246 - 3.374D + 6.224D^2 - 3.488D^3 \end{aligned}\right\} \tag{93}$$

$$R_3 = 1.8 \text{ kgf/cm}^3 \quad \left.\begin{aligned} C &= 0.588 - 0.262D + 0.542D^2 - 0.301D^3 \\ \alpha &= 0.00087 + 0.0186D - 0.0599D^2 + 0.0596D^3 \\ \beta &= 1.160 + 3.335D - 1.693D^2 + 1.396D^3 \end{aligned}\right\} \tag{94}$$

$$R_3 = 6.0\ \text{kgf/cm}^3 \quad \left.\begin{array}{l} C = 0.602 - 0.303D + 0.694D^2 - 0.390D^3 \\ \alpha = -0.00258 + 0.0349D - 0.0714D^2 + 0.0567D^3 \\ \beta = 2.805 - 4.669D + 6.510D^2 - 3.476D^3 \end{array}\right\} \quad (95)$$

where D is the diameter of the pipe.

For the other radial spring constants and widths, we can use these nine formulas and linear interpolation.

Fig. 20 through **Fig. 25** show the calculation results by means of shell model-I, shell model-II and formula Eq. (86).

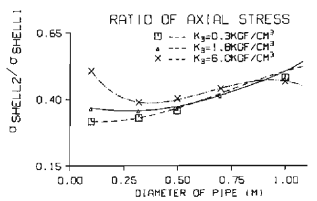

Fig. 20 Axial stress ratio. (witdth of differential settlement= 5 m, critical relative displacement= 2 cm)

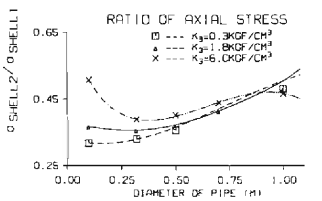

Fig. 21 Axial stress ratio. (width of differential settlement= 5 m, critical relative displacement= 4 cm)

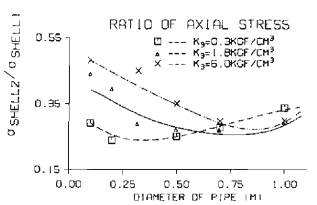

Fig. 22 Axial stress ratio. (width of differential settlement= 10 m, critical relative displacement= 2 cm)

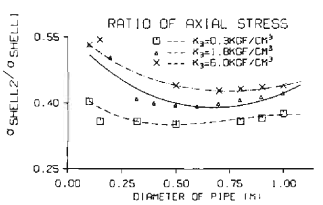

Fig. 23 Axial stress ratio. (width of differential settlement= 10 m, critical relative displacement= 4 cm)

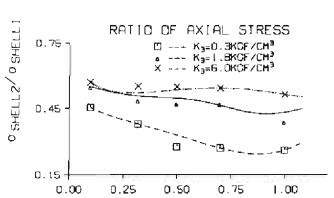

Fig. 24 Axial stress ratio. (width of differential settlement= 20 m, critical relative displacement= 2 cm)

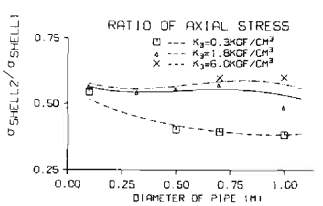

Fig. 25 Axial stress ratio. (width of differential settlement= 20 m, critical relative displacement= 4 cm)

4. Conclusions

From the above observations, the following conclusions can be drawn :

(1) Program SMFABP (Shell Model-FMA Analysis of Buried Pipeline) developed in

this study is appropriate for the calculation of buried pipelines subjected to sinusoidal waves, differential settlement and ground dislocation.

(2) The distribution of earth pressure has great influence on the stresses of buried pipelines subjected to transverse ground deformation. In this case, shell model-II presented in this paper is apparently powerful while beam models and shell model-I are not suitable because they can not properly take this contribution into account.

(3) Differential settlement, which is still not fully taken into account in most of the design codes of buried pipelines, appears to be the most threatening loading because it can generate large stresses than other kinds of loads.

(4) The distortion of the cross section of pipelines does occur when they are subjected to transverse ground deformation. Nevertheless, stresses due to such distortion are small for the common pipe under common ground conditions. The effect of this distortion may become significant only when the pipe is very thin or the ground is very stiff.

(5) In the case of axial ground deformation loading, the beam model and shell model give approximately the same results.

(6) Axial stress is usually more significant than the circumferential one. However circumferential stress becomes significant if the pipe is subjected to the transverse deformation of stiff ground.

(7) The stiffness of radial spring is a significant factor in the analysis of pipelines under transverse ground deformation. Nevertheless, very few data on radial spring constant exists. More work on this appears necessary.

This paper concentrates on straight continuous pipelines. However most of the conclusions can apparently be extended to jointed or bent pipelines. The analysis method developed in this paper is considered to be stable not only for the analysis of buried pipelines, but also for the analysis of other structures such as steel piles and so on.

Acknowledgment

The authors wish to extend their deep appreciation to Prof. Koichi Akai of Kyoto University for his valuable suggestions and encouragement throughout this study. The numerical computation for this work has been made on FACOM M-780/30/VP-400E/VP-200 computer system of the Data Processing Center, Kyoto University.

References

1) S. Takata, "Seismic response analysis of buried PVC and ductile iron pipelines", Recent Advances in Lifeline Earthquake Engineering in Japan, edited by Heki Shibata (1980).
2) S. Takata, K. Tanabe "Three-dimensional seismic response analysis of buried continuous or jointed pipelines", Transactions of the ASME, 80/Vol. 109, February 1987.
3) M. Shinozuka, T. Koike, "Estimation of structural strain in underground lifeline pipes", Lifeline Earthquake Engineering-Buried Pipelines, Seismic Risk, and Instrumentation, Edited by T. Ariman, S. C. Liu and E. Nickell.
4) Japan Gas Association "Earthquake resistant design guideline for gas pipelines", 1979.

5) M. Novak and A. Hindy, "Seismic analysis of underground tubular structure", Proceedings of the 7th World Conference on Earthquake Engineering, Sep. 8-13 Vol. 8, 1980, pp. 287-294.
6) S. K. Datta, "Dynamic behavior of a buired pipe in a seismic environment", Journal of Allied Mechanics, March 1982, Vol. 49/141.
7) S. K. Datta, "Dynamic response of pipelines to moving load", Earthquake Engineering and Structural Dynamics, Vol. 12, 59-72 (1984).
8) T. Chakraborty, "Forced vibration of continuous pipelines due to propagation seismic loads", M. S. Thesis, Department of Mechanical Engineering, University of Cclorado, 1983.
9) S. Kawamata, "Shell structure enalysis", Structural Engineering Lecture Based on Computer II-6-A.
10) J. H. Percy, T. H. H. Pian & D. R. Navaratna "Application of matrix displacement method to linear elastic analysis of shell of revolution", AIAA J. 3 2138-1245 (1965).
11) J. A. Strick, D. R. Navaratna & t. H. H. Pian, "Improvements on the analysis of shells of revolution by the matrix displacement method", AIAA Journal, Vol. 4, No. 11, 2069-2072 (1966).
12) D. R. Navaratna, T. H. H. Pian & E. A. Witmar, "Stability analysis of shell of revolution by the matrix displacement method", AIAA Journal, Vol. 6 No. 2, 355-361 (1968).
13) J. A. Sticklin, W. E. Haisler, H. R. McDougall & F. J. Stebbins, "Nonlinear analysis of shell of revolution by the displacement method", AIAA Journal, Vol. 6, No. 12, 2306-2312 (1986).
14) A. Sakurai, T. Takahashi, C. Kurihara & H. Yajina, "Earthquake resistant of buried pipelines based on ground strains", Technical Report No. 69087, Central Research Institute of Electric Power Industry, 1970, pp 1-58.
15) Japanese Association of Water Works, "Guideline and interpretation for earthquake resistant construction of water structures".
16) O. C. Zienkiewicz, "The finite element method", McGraw-Hill Book Company (UK) Limited.
17) H. Goto, M. Sugito, H. Kameda & Y. Ishikawa, "Seismic response analysis of joint-connected buried pipeline including bent section", the Memoirs of the Faculty of Engineering, Kyoto University, Vol. XLIV, Part 1, Jan, 1982.
18) H. Nakamura, "A modified transfer matrix method with improved round off errors", Proceedings, JSCE, Sept, 1979, pp. 43-53.
19) H. Kameda, M. Sinozuka, "Simplified formula for axial strains of buried pipes induced by propagating seismic waves", Memoirs of the Faculty of Engineering, Kyoto University, Vol. XLIV, Part 2, Apr., 1982.

Appendix A: Formulas

$$[B]=\begin{vmatrix} -1/L & 0 & 0 & 0 \\ 0 & n(1-\varepsilon)/r & (1-3\xi^2+2\xi^3)/r & L(\xi-2\xi^2+\xi^3)/r \\ -n(1-\xi)/r & -1/L & 0 & 0 \\ 0 & 0 & (6-12\xi)/L^2 & (4-6\xi)/L \\ 0 & n(1-\xi)/r^2 & n^2(1-3\xi^2+2\xi^3)/r^2 & n^2L(\xi-2\xi^2+\xi^3)/r^2 \\ 0 & -2/rL & -12n(\xi+\xi^2)Lr & 2n(1-4\xi+3\xi^2)/r \end{vmatrix}$$

$$\begin{vmatrix} 1/L & 0 & 0 & 0 \\ 0 & n\xi/r & (3\xi^2-2\xi^3)/r & -L(\xi^2-\xi^3)/r \\ -n\xi/r & 1/L & 0 & 0 \\ 0 & 0 & -(6-12\xi)/L^2 & (2-6\xi)/L^2 \\ 0 & n\xi/r^2 & n^2(3\xi^2-2\xi^3)/r^2 & -n^2L(\xi^2-\xi^3)/r^2 \\ 0 & 2/Lr & 12n(\xi-\xi^2)rL & -2n(2\xi-3\xi^2)/r \end{vmatrix} \quad \cdots\cdots\text{(A-1)}$$

$$[B_0]=\left|\begin{array}{ccc:ccc} -1/L & 0 & 0 & 1/L & 0 & 0 \\ 0 & (1-3\xi^2+2\xi^3)/r & L(\xi-2\xi^2+\xi^3)/r & 0 & (3\xi^2-2\xi^3)/r & -L(\xi^2-\xi^3)/r \\ 0 & (6-12\xi)/L^2 & (4-6\xi)L & 0 & -(6-12\xi)/L^2 & (2-6\xi)/L^2 \end{array}\right| \quad \cdots\cdots\text{(A-3)}$$

$$[N]^T[kn][N]=$$

$$\begin{pmatrix} k_x(1-\xi)^2 & & & & & & & \\ 0 & k_\theta(1-\xi) & & & \text{symmetry} & & & \\ 0 & 0 & k_x(1-3\xi^2+2\xi^3)^2 & & & & & \\ 0 & 0 & k_xL(\xi-2\xi^2+\xi^3)^2*(1-3\xi^2+2\xi^3) & k_xL^2(\xi-2\xi^2+\xi^3)^2 & & & & \\ k_x(1-\xi) & 0 & 0 & 0 & k_x\xi^2 & & & \\ 0 & k_\theta\xi(1-\xi) & 0 & 0 & 0 & k_\theta\xi^2 & & \\ 0 & 0 & k_x(3\xi^2-2\xi^3)*(1-3\xi^2+2\xi)^3 & kL_x(3\xi^2-2\xi^3)*(\xi-2\xi^2+\xi^3) & 0 & 0 & k_x(3\xi^2-2\xi^3)^2 & \\ 0 & 0 & -kL_x(\xi^2-\xi^3)*(1-3\xi^2-2\xi^3) & -k_xL^2(\xi^2-\xi^3)*(\xi-2\xi^2+\xi^3) & 0 & 0 & -k_xL(\xi^2-\xi^3)*(3\xi^2-2\xi^3) & k_xL^2(\xi^2-\xi^3)^2 \end{pmatrix} \quad \cdots\cdots\text{(A-2)}$$

(A-4)

$$\begin{aligned}
f_2 &= -\cos\omega(t-x_i\cos\alpha/c)c/\omega-\sin\omega(t-(x_i+L_i)\cos\alpha/c)c^2/(\omega^2L_i)\\
&\quad+\sin\omega(t-x_i\cos\alpha/c)c^2/(\omega^2L_i)\\
f_3 &= -\cos\omega(t-x_i\cos\alpha/c)c/\omega-6\cos\omega(t-(x_i-L_i)\cos\alpha/c)c^3/(\omega^3L_i^2)\\
&\quad-6\cos\omega(t-x_i\cos\alpha/c)c^3/(\omega^3L_i^2)-12\sin\omega(t-(x_i+L_i)\cos\alpha/c)c^4/(\omega^4L_i^3)\\
&\quad+12\sin\omega(t-x_i\cos\alpha/c)c^4/(\omega^4L_i^3)\\
f_4 &= -\sin\omega(t-x_i\cos\alpha/c)c^2/(\omega^2L_i)-2\cos\omega(t-(x_i-L_i)\cos\alpha/c)c^3/(\omega^3L_i^2)\\
&\quad-4\cos\omega(t-x_i\cos\alpha/c)c^3/(\omega^3L_i^2)-6\sin\omega(t-(x_i+L_i)\cos\alpha/c)c^4/(\omega^4L_i^3)\\
&\quad+6\sin\omega(t-x_i\cos\alpha/c)c^4/(\omega^4L_i^3)\\
f_6 &= \cos\omega(t-(x_i-L_i)\cos\alpha/c)c/\omega+\sin\omega(t-(x_i+L_i)\cos\alpha/c)c^2/(\omega^2L)\\
&\quad-\sin\omega(t-x_i\cos\alpha/c)c^2/(\omega^2L_i)\\
f_7 &= \cos\omega(t-(x_i-L_i)\cos\alpha/c)c/\omega+6\cos\omega(t-(x_i-L_i)\cos\alpha/c)c^3/(\omega^3L_i^2)\\
&\quad+6\cos\omega(t-x_i\cos\alpha/c)c^3/(\omega^3L_i^2)+12\sin\omega(t-(x_i+L_i)\cos\alpha/c)c^4/(\omega^4L_i^2)\\
&\quad-12\sin\omega(t-x_i\cos\alpha/c)c^4/(\omega^4L_i^2)\\
f_8 &= -\sin\omega(t-(x_i+L_i)\cos\alpha/c)c^2/(\omega^2L_i)+4\cos\omega(t-(x_i-L_i)\cos\alpha/c)c^3/(\omega^3L_i^2)\\
&\quad+2\cos\omega(t-x_i\cos\alpha/c)c^3/(\omega^3L_i^2)+6\sin\omega(t-(x_i+L_i)\cos\alpha/c)c^4/(\omega^4L_i^3)
\end{aligned}$$

Loading Vector of SV Wave

For $n=0$, $\{P_0\}=[P_1, P_2, P_3, P_4, P_5, P_6]$
in which

$$\text{(A-5)}\begin{cases} P_1=-k_s a_0 f_2 \sin\alpha \\ P_2=W_0(x)f_3 \\ P_3=W_0(x)Lf_4 \\ P_4=-k_s a_0 f_6 \sin\alpha \\ P_5=W_0(x)f_7 \\ P_6=-W_0(x)Lf_8 \end{cases}$$

For $n=1$, $\{P_1\}=[P_1, P_2, P_3, P_4, P_5, P_6, P_7, P_8]$
here

$$\text{(A-6)}\begin{cases} P_1=P_5=0 \\ P_2=-a_0 k\, f_2 \cos\alpha \\ P_3=W_1(x)f_3 \\ P_4=W_1(x)Lf_4 \\ P_6=-a_0 k\, f_6 \cos\alpha \\ P_7=W_1(x)f_7 \\ P_8=-W_1(x)Lf_8 \end{cases}$$

For $n=2, 4, 6, 8, 10$, $\{P_n\}=[P_1, P_2, P_3, P_4, P_5, P_6, P_7, P_8]$
were

$$\text{(A-7)}\begin{cases} P_1=P_5=0 \\ P_2=0 \\ P_3=W_n(x)f_3 \\ P_4=W_n(x)Lf_4 \\ P_6=0 \\ P_7=W_n(x)f_7 \\ P_8=-W_n(x)Lf_8 \end{cases}$$

$W_n(x)$ are as follows:
if $\sin\omega(t-x\cos\alpha/c)>0$, then

$$\text{(A-8)}\begin{cases} W_0(x)=a_0\sin\alpha\sin\omega(t-x\cos\alpha/c)/\pi \\ W_1(x)=a_0\sin\alpha\sin\omega(t-x\cos\alpha/c)/2 \\ W_2(x)=2a_0\sin\alpha\sin\omega(t-x\cos\alpha/c)/(3\pi) \\ W_4(x)=-2a_0\sin\alpha\sin\omega(t-x\cos\alpha/c)/(15\pi) \\ W_6(x)=2a_0\sin\alpha\sin\omega(t-x\cos\alpha/c)/(35\pi) \\ W_8(x)=-2a_0\sin\alpha\sin\omega(t-x\cos\alpha/c)/(63\pi) \\ W_{10}(x)=2a_0\sin\alpha\sin\omega(t-x\cos\alpha/c)/(99\pi) \end{cases}$$

otherwise,

$$\text{(A-9)}\begin{cases} W_0(x)=-a_0\sin\alpha\sin\omega(t-\cos\alpha/c)/\pi \\ W_1(x)=a_0\sin\alpha\sin\omega(t-x\cos\alpha/c)/2 \\ W_2(x)=-2a_0\sin\alpha\sin\omega(t-x\cos\alpha/c)/(3\pi) \\ W_4(x)=2a_0\sin\alpha\sin\omega(t-x\cos\alpha/c)/(15\pi) \\ W_6(x)=-2a_0\sin\alpha\sin\omega(t-x\cos\alpha/c)/(35\pi) \\ W_8(x)=2a_0\sin\alpha\sin\omega(t-x\cos\alpha/c)/(63\pi) \\ W_{10}(x)=-2a_0\sin\alpha\sin\omega(t-x\cos\alpha/c)/(99\pi) \end{cases}$$

Loading Vector of Dislocation

For $n=0$, $\{P_0\}=[P_1, P_2, P_3, P_4, P_5, P_6]$
in the connected element,

$$\text{(A-10)}\begin{cases} P_1=k_x a_0 L\cos\alpha/6 \\ P_2=3k_x a_0 L\sin\alpha/(20\pi) \\ P_3=k_x L^2 a_0\sin\alpha/(30\pi) \\ P_4=k_x a_0 L\cos\alpha/3 \\ P_5=7k_x a_0 L\sin\alpha/(20\pi) \\ P_6=-k_x L^2 a_0\sin\alpha/(20\pi) \end{cases}$$

in the right part,

$$\text{(A-11)}\begin{cases} P_1=k_x a_0 L\cos\alpha/2 \\ P_2=k_x a_0 L\sin\alpha/(2\pi) \\ P_3=k_x L^2 a_0\sin\alpha(12\pi) \\ P_4=k_x a_0 L\cos\alpha/2 \\ P_5=k_x a_0 L\sin\alpha/(2\pi) \\ P_6=-k_x L^2 a_0\sin\alpha/(12\pi) \end{cases}$$

For $n=1$, $\{P_1\}=[P_1, P_2, P_3, P_4, P_5, P_6, P_7, P_8]$
in the connected element,

$$\text{(A-12)}\begin{cases} P_1=P_5=0 \\ P_2=k\ a_0 L\cos\alpha/6 \\ P_3=3k_x a_0 L\sin\alpha/40 \\ P_4=k_x L^2 a_0\sin\alpha/60 \\ P_6=k\ a_0 L\cos\alpha/3 \\ P_7=7k_x a_0 L\sin\alpha/40 \\ P_8=-k_x L^2 a_0\sin\alpha/40 \end{cases}$$

in the right part,

$$\text{(A-13)}\begin{cases} P_1=P_5=0 \\ P_2=k\ a_0 L\cos\alpha/2 \\ P_3=k_x a_0 L\sin\alpha/4 \\ P_4=k_x L^2 a_0\sin\alpha/24 \\ P_6=k\ a_0 L\cos\alpha/2 \\ P_7=k_x a_0 L\sin\alpha/4 \\ P_8=-k_x L^2 a_0\sin\alpha/24 \end{cases}$$

For $2k=n=2, 4, 6, 8, 10$, $\{P_n\}=[P_1, P_2, P_3, P_4, P_5, P_6, P_7, P_8]$
in the connected element,

$$\text{(A-14)}\begin{cases} P_1=P_5=P2=P6=0 \\ P_3=3(-1)^{k+1}k_x a_0 L\sin\alpha/(10\pi(4k^2-1)) \\ P_4=(-1)^{k+1}k_x a_0 L\sin\alpha/(15\pi(4k^2-1)) \\ P_7=7(-1)^{k+1}k_x a_0 L\sin\alpha/(10\pi(5k^2-1)) \\ P_8=(-1)^k k_x a_0 L\sin\alpha/(15\pi(4k^2-1)) \end{cases}$$

in the right part,

$$\begin{cases} P_1=P_5=P2=P6=0 \\ P_3(-1)^{k+1}k_x a_0 L \sin\alpha/(\pi(4k^2-1)) \\ P_4=(-1)^{k+1}k_x a_0 L \sin\alpha/(6\pi(4k^2-1)) \\ P_7=(-1)^{k+1}k_x a_0 L \sin\alpha//(\pi(4k^2-1)) \\ P_8=(-1)^{k}k_x a_0 L \sin\alpha/(6\pi(4k^2-1)) \end{cases}$$

Loading Vector of Different Settlement

The loading vetors of different settlement are the same as those of the seismic wave in the differential settlement area due to the assumption that differential settlement occur in the shape of half wave length of a sinnusoidal wave, but become zero in other parts.